ACS OMEGA

Article

Cite This: ACS Omega 2018, 3, 266−272

Thermodynamic Model for Quantum Dot Assemblies Formed Because of Charge Transfer

Rekha Mahadevu and Anshu Pandey*

Solid State and Structural Chemistry Unit, Indian Institute of Science, Bangalore 560012, India

Supporting Information

ABSTRACT: Two initially neutral semiconductor quantum dots with appropriate band offsets can participate in a ground state charge transfer process. The charge transfer manifests itself in the form of bleaching of optical transitions and also causes the quantum dots to precipitate from solution, giving rise to assemblies with unusual properties. As this represents a postsynthetic modification of the electronic structure of quantum dots, it holds tremendous potential for improving the characteristics of quantum dot devices. Here, we study the dependencies of the properties of these assemblies on the structure of the participating quantum dots. In particular, we find that for assemblies formed out of Cu:CdS and ZnTe/CdS quantum dots, the composition of the assembly varies from 1:1.26 to 1:0.23 ZnTe/CdS to Cu:CdS as the shell thickness of CdS in ZnTe/CdS is increased. In contrast, the composition changes from 1:1.1 to 1:15 for PbSe/CdSe and Cu:CdS quantum dots, as the size of the PbSe core is increased. These observations are explained on the basis of a phenomenological thermodynamic model. The applicability of thermodynamics to this example of self-assembly is verified empirically.

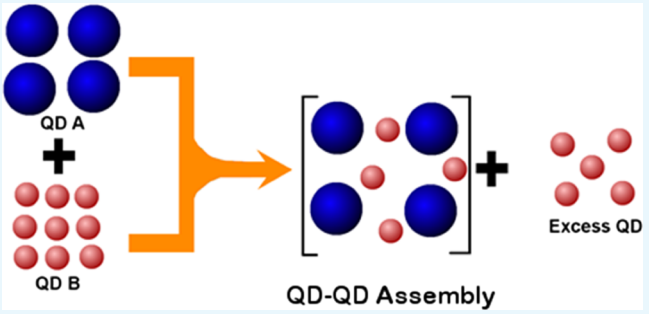

INTRODUCTION

The electronic states of semiconductor quantum dots (QDs) can be engineered in numerous ways. While the design of core/shell architectures enables precise control over wave functions,[1−4] the intentional inclusion of dopants allows for the introduction of custom electronic states. In this regard, ground-state charge transfer between QDs offers the potential of a postsynthetic modification of QD opto-electronic properties[5,6] and is therefore of significant interest to the preparation of QD devices.[4,7−16]

A typical example of such a charge transfer is shown in the schematic (Figure 1a). This involves a QD that contains a suitable donor or acceptor level, and another QD that is capable of accepting/donating charges from/to that level. The simplest example involves a copper containing QD (e.g., Cu:CdS or Cu:ZnSe/CdSe[17]) and another QD based on PbSe[18] or ZnTe.[19] In a previous publication, we showed this process to be a ground-state effect, and no measurable influence of light on the process could be identified.[20] We note that a ligand shell is expected to lead to hopping times ∼0.1 μs.[21] Thick (1 nm) electron-confining shells (e.g., with an offset of 1 eV) may slow down tunneling rates further by five orders of magnitude. The electron tunnel time in these circumstances is in the order of 10^{-2} s, which is sufficient to allow effective charge transfer and equilibration over the timescale of assembly formation (10−1000 s).

Following this charge transfer, the two participating QDs become oppositely charged and precipitate from solution, forming an assembly. While such assemblies lack a crystalline order,[20] these show other properties that indicate that these are a thermodynamic end product. Qualitative indications of a thermodynamic equilibrium are evidenced in the existence of a well-defined macroscopic morphology.[22,23] Figure 1b shows the transmission electron microscopy (TEM) images where a peculiar barrel-like assembly of over a million QDs is observed.

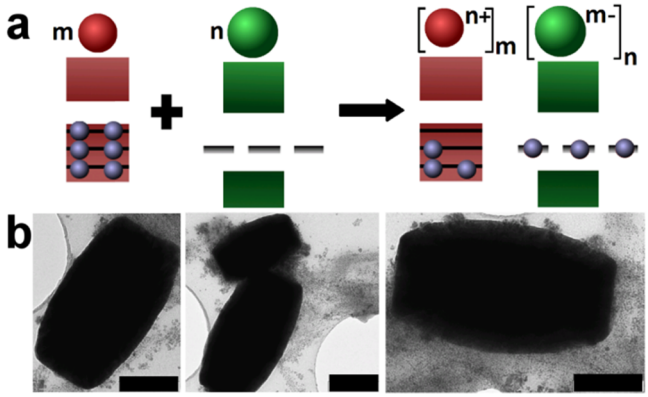

Figure 1. (a) Schematic of QDs reacting to form a Coulomb-bound assembly. (b) TEM images of Coulomb-bound assemblies formed out of PbSe/CdSe and Cu:CdS QDs. Each barrel is an assembly of over 10^6 QDs. Scale bars are 100 nm.

Received: October 5, 2017
Accepted: December 25, 2017
Published: January 10, 2018

DOI: 10.1021/acsomega.7b01486
ACS Omega 2018, 3, 266−272

The ability of a large ($>10^6$) number of QDs to spontaneously seek such peculiar, macroscopically symmetric configurations provides a strong, though qualitative suggestion regarding the thermodynamic nature of the assembly process. Other assembly morphologies are exemplified in Figure S1. Presently, we are unaware of the parameters responsible for size and shape of the assembly. Assemblies with the same composition do end up showing different morphologies, and it is therefore inferred that composition is not the primary parameter guiding the assembly shape. It is feasible that different shapes arise from different nuclei; however, the nucleation process of these assemblies is unclear at the moment. The assemblies thus formed bear some resemblance to charged granular solids reported by other researchers.[24−27]

Here, we study the influence of the QD structure on the properties of the assemblies. To extract useful parameters relating to the assembly formation process, we first show that the assembly process is ultimately determined by thermodynamics, despite the lack of a crystalline order. Such assemblies can therefore be likened to liquids in that these lack structure but are characterized by well-defined thermodynamic parameters. It is further shown that the assembly formation process has a remarkable ability to seek the free-energy minimum even when the process is initiated from vastly different starting positions of the free-energy landscape. We explain the robustness of the assembly formation process in terms of a phenomenological thermodynamic model. Specific predictions of the model regarding the effects of the QD size and structure on assembly composition are validated experimentally. Finally, the model is used to estimate the free-energy penalty associated with the creation of an error in composition. The strong (∼1 eV per composition defect) energy penalty associated with creation of composition errors explains the existence of a fixed characteristic composition for this type of the QD assembly.

RESULTS AND DISCUSSIONS

Assemblies of QDs were prepared using a procedure similar to the one reported previously.[20] QDs were initially prepared using the techniques described in the Supporting Information. Both the QD participants in the assembly process were separated from the original solutions by precipitation using ethanol. Subsequently, QDs were redispersed in hexane, and any hexane-insoluble components of the original solution are separated out. Subsequently, the QDs are again precipitated by the addition of alcohols. These steps of dissolution and reprecipitation are typically undertaken three to five times to obtain an optically clear dispersion of QDs free from unbound ligands and reaction byproducts. If kept aside, such dispersions are stable for a time period in excess of a week in the dark. Following the cleaning steps, the two dispersions of QDs from which the assembly is to be constructed are mixed. Following mixing, precipitation of the assembly is observed within ∼1 h of standing. The instability exhibited by the combination of QDs is in contrast to the stability of the individual QD dispersions. This process may be accelerated by first evaporating the solvent at room temperature, and subsequently adding fresh solvent. In either case, it is observed that the precipitation is selective, and a fraction of QDs remain behind in the solution.

The QD assembly is separated from the unbound, solvent-dispersed QDs by decantation followed by several rounds of washing with hexane. The assembled and unbound QDs are then dried separately and analyzed further. The total amount of QDs was inferred by adding the amounts of bound and unbound material.

VALIDITY OF THERMODYNAMIC MODELS

In most cases, the attainment of a crystalline state is used to justify the applicability of thermodynamics to an assembly process.[28−30] While this is a robust criterion in several cases, it is certainly feasible that a crystalline state may not be the thermodynamic ground state for a granular solid with arbitrarily complex interactions. Alternate criteria such as the possibility of attainment of a definite morphology do qualitatively suggest that the assembly is governed by thermodynamics;[25,31−34] however, a more quantitative criterion is desirable. We therefore studied the composition of the assembly formed from the QDs to ascertain the applicability of thermodynamics in the process.

It is known that the composition of the QD assembly is largely independent of the starting quantities of QDs. The results of a typical experiment are exemplified in Figure 2a. This figure shows the variation in the ratio of the QDs (1:y) present in assemblies as a function of the ratios in which they were taken initially. Even though the initial ratios of the QDs are changed from 1:3 to 1:15, the stoichiometry is relatively constant at $1:(1.8 \pm 0.3)$. Thus, there is no bearing of the initial ratios of the QDs on the stoichiometry of the end product. This implies the existence of a robust mechanism by which QD assemblies exclude the excess of one type of QD whenever there is a deficit of the partnering dot. From a thermodynamic perspective, this implies a unique free-energy minimum, as well as consistent ability of the system to seek out this minimum under experimental conditions.

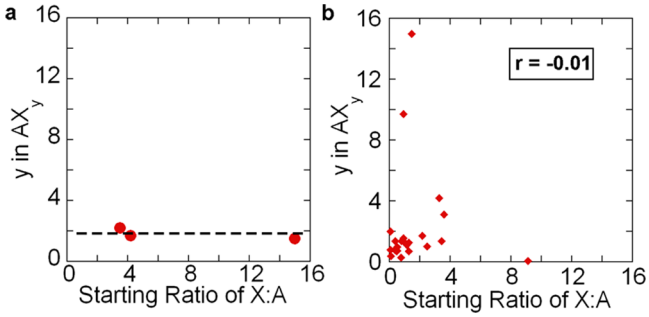

Figure 2. (a) Stoichiometry of Coulomb-bound assemblies formed between two QDs when the ratios of the participants are changed. These data have been taken from ref 20. (b) Stoichiometries of various Coulomb-bound assemblies as a function of starting ratios of QDs. r is the Pearson correlation of this data set.

A more quantitative view is presented in Figure 2b. This figure shows the data collected from 24 different assemblies prepared from different sizes and formulations of QDs. This figure uses Cu:CdS or Cu:ZnSe/CdSe mixed with PbSe- and ZnTe-based core/shell QDs. Each QD pair has been combined together twice with a pseudo-random starting ratio of the participating QDs. The observed composition ratio of the assembly is plotted along the y axis, and the initial ratios of the participating QDs are plotted along the x axis. Because of the different types of QDs employed in the assembly preparation, the observed composition varies widely from 0.06 to 15. At the same time, the initial ratio of the participating QDs also changes widely over a similar range, from 0.05 to 9 over the entire data set. Even though both parameters change over a

DOI: 10.1021/acsomega.7b01486
ACS Omega 2018, 3, 266−272

very similar range of values, the lack of correlation between these two parameters is immediately apparent. The Pearson correlation for this scatter plot is observed to be −0.01. The near-zero value of the Pearson correlation implies that the final stoichiometry of the assembly is completely unrelated to the starting ratios of QDs and confirms the existence of a thermodynamically controlled mechanism of assembly formation. Stated in terms of free energy, the chemical potentials of QDs in solutions used to prepare the assembly differ from the ideally required chemical potentials $\Delta\mu = \mu_{used} - \mu_{required} = RT \ln(a_{used}/a_{required})$ by upto 12 kJ/mol in certain cases. The ability of the assembly process to lead to a unique final composition despite the strong contrary bias provided by the chemical potential thus implies ergodicity and the validity of equilibrium thermodynamics for the type of assembly described here.

THERMODYNAMIC MODEL FOR ASSEMBLY FORMATION

The Born−Haber cycle is frequently employed to describe the thermodynamics of ionic compounds. As the interactions guiding the assembly process are Coulombic, we adopt a similar model. For simplicity, we first consider an assembly where QDs occur in a 1:1 ratio. Assemblies that contain a different ratio of the two QDs can be described through straightforward extensions that are presented later.

The Born−Haber cycle explicitly considers the sublimation and/or the dissociation of the original elements, the ionization energy and the electron affinity, and finally the lattice energy.

Because of the absence of an underlying lattice structure, it is further convenient to assume that the assembly comprises pairs of QDs. In the case of the QD assembly process, individual QDs start off in their neutral state in an organic solvent, and thus sublimation-/dissociation-like terms are absent. The ionization energy and electron affinity terms can be replaced by equivalent terms for QDs. In the strong confinement regime in particular, it is convenient to split this contribution into three terms, namely, the offsets present in the bulk semiconductor, the confinement energy, and lastly the Coulomb energy because of charge transfer. Finally, it is necessary to include a term corresponding to lattice energy that accounts for the interactions of the remainder assembly with a pair of QDs.

We can thus write an expression for the energy of a 1:1 assembly for transfer of n electrons $(\Delta E_{n,1})$

$$nP + \epsilon + \frac{n^2}{ca_+} + \frac{n^2}{c'a_-} - \frac{n^2}{c''r} + C_{av} = \Delta E_{n,1} \quad (1)$$

Here, P is the potential arising from offsets between uncharged bulk materials that make up the QDs, n is the number of electrons transferred between the QDs, c, c'', c', are constants related to the medium dielectric constant, r is the inter QD separation, ϵ is the change in confinement energy of the electrons when they are transferred from one QD to another, while $a_\pm$ are the radii of the charged regions of the two QDs. C_{av} is the interaction energy of a pair of QDs with the remaining assembly. In a typical assembly, Coulomb terms are similar in magnitude, while the confinement term is typically smaller. For example, $P \approx -0.5$ eV for ZnTe/CdS−Cu:CdS. For $n \approx 10$ and a dielectric constant of 10, the charging terms are also individually as large as 1 eV. The confinement energy per charge $\epsilon/n \approx 0.01$−0.5 eV depending on the QD size and charging level. Thus, it is evident that the assembly formation process is guided largely by classical effects while quantum mechanics plays a relatively minor role.

The criterion for the amount of charge transferred can be arrived by setting $\frac{\partial \Delta E_{n,1}}{\partial n} = 0$, which yields $P + \dot{\epsilon} + \frac{2n}{ca_+} + \frac{2n}{c'a_-} - \frac{2n}{c''r} + \dot{C}_{av} = 0$ as the criterion for the number of electrons transferred in a 1:1 solid.[35] As further shown in the Supporting Information, it is possible to write an approximate form of these equations for a 1:$(1 + x)$ solid, where x is a small number. In particular, we obtain

$$nP - \frac{n^2}{cr} + \in + \frac{n^2}{ca_+} + \frac{n^2}{(1+x)ca_-} + \frac{n^2}{(1+x)cd} + C_{av} = \Delta E_{n,1+x}$$

To simplify the discussion, here c is any one of the constants related to the medium dielectric; details are presented in the Supporting Information. The validity of this model may be verified empirically by examining the behavior of this model under different perturbations. We first consider the situation where the distances between QDs are increased gradually. The magnitude of the offsite stabilization term, $-\frac{n^2}{cr}$, decreases, while the onsite repulsions, $\frac{n^2}{ca_+}$ and $\frac{n^2}{ca_-}$, are unchanged. Both QDs participating in the assembly process are affected differently by changes in these terms, and this causes a deviation from a 1:1 participation of both QDs. As shown in the Supporting Information, it is possible to extract the relationship $y = E + \frac{F}{r}$ to describe changes in the chemical composition of the assembly induced because of changes in the distances between QDs. Here, y is the stoichiometric ratio of the positively charged QD to the negatively charged QD. r is the interparticle separation and E and F are fitting parameters. This expression shows the relative importance of classical, interparticle Coulomb interactions in deciding the composition of the assembly.

The continuous tuning of interparticle separations in a QD assembly can be implemented using core/shell QD structures. In the case of the ZnTe/CdS system, the high CdS valence band offset ensures that holes remain largely localized to the ZnTe core.[19] Figure 3a employs an effective mass approach to estimate the confinement energies of holes at the ZnTe band edge due to growth of a CdS spacer. This calculation employs parameters used earlier to describe the ZnTe/CdS system.[19] Shell growth is considered to occur over a core of a radius of 2 nm. As shown in this Figure 3a, increasing thickness of the CdS shell thus does not cause significant changes in the properties of electronic states in the vicinity of the ZnTe valence band top (Figure 3a, black curve).

In contrast, the band edge exciton energy (Figure 3a, blue curve) changes as a consequence of CdS shell growth, primarily because of a change in electron confinement (Figure 3a, red curve). Increasing the CdS shell thickness thus increases the distance between electronic states of the participating QDs without significantly changing the density of single-particle levels at the valence band edge. Thus, a study of assemblies formed out of QDs with different CdS shell thicknesses provides the same information as the effect of variation of changing inter-QD separation in a single assembly. The effects of increased QD separation on the Coulomb interaction terms are shown in Figure 3b. Because holes are primarily localized to

DOI: 10.1021/acsomega.7b01486
ACS Omega 2018, 3, 266−272

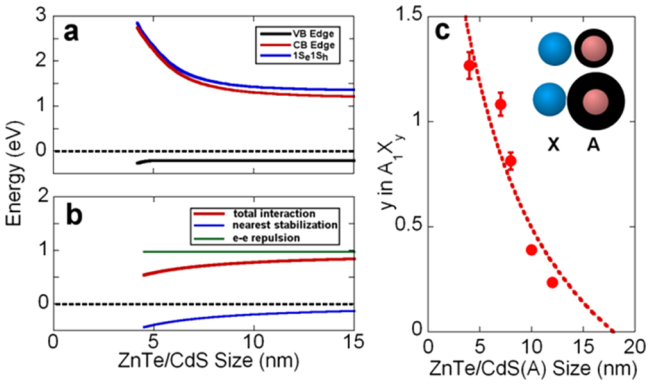

Figure 3. (a) Energy of the ZnTe/CdS valence band edge (black), conduction band edge (red), and band edge excitonic energy (blue) for a 2 nm ZnTe QD as a function of the total QD diameter. (b) Variation of onsite electron−electron repulsion (green), nearest neighbor stabilization (blue), and total Coulomb interaction per electron (red) as a function of the total QD diameter. This estimate assumes the total charge per QD to be constant. (c) Variation of stoichiometry of ZnTe/CdS(A) + Cu/CdS(X) QD assemblies as a function of QD A diameter.

the ZnTe core, the Coulomb charging energy (Figure 3b, green curve) does not change as a function of shell thickness. However, the Coulomb stabilization due to oppositely charged nearest neighbors (Figure 3b, blue curve) decreases in magnitude as the CdS shell thickness is increased because of an increase in inter-QD separation. From a Coulomb stabilization viewpoint, the system thus becomes less suitable for charge transfer as the CdS shell thickness is increased (Figure 3b, red curve). As shown in Figure 3c, with increasing thickness of the CdS shell, the amount of Cu:CdS (QD X) in the assembly decreases relative to the amount of ZnTe/CdS (QD A). The error bars in Figure 3c represent the range of compositions observed when two nominally identical batches of Cu:CdS QDs are combined with ZnTe/CdS QDs. Each data point corresponds to the average. The expression for composition as predicted by the model can be recast in a slightly different form to better describe this experiment. We note that the inter-QD distance is the sum of the individual QD radii and any intermediate ligands. Thus, $r = r_+ + G$ and $y = E + \frac{F}{r_+ + G}$. Here, r_+ is the total radius of the ZnTe/CdS QD. The parameter G represents the radius of the other participating dot as well as the additional separation caused because of the ligand shell. The other participating QD has a 2.5 nm radius, while the ligand shell itself contributes approximately 0.5 nm. We thus take G = 3 nm; only the parameters E and F are allowed to vary during the fitting. As shown in Figure 3c, this provides a reasonable description of the data, thereby confirming the validity of the proposed model for the assembly process.

It is further necessary to consider the validity of this model in cases where the quantum confinement effects have a small but nonnegligible influence on the assembly. As smaller QDs have progressively larger values of confinement, we considered the compositions of assemblies comprising Cu:CdS- and PbSe-based QDs. The sizes of the PbSe/CdSe QD core is varied through this experiment. For very small QDs, the confinement energy increases with the inverse square of the radius and reduces the ability of small PbSe QDs to effectively participate in the assembly. For very large PbSe particles, a single particle can form an assembly with a large number of Cu:CdS QDs, essentially limited by the QD size.

To explore this further, we synthesized assemblies formed by Cu:CdS- and PbSe-based QDs. All PbSe QDs, barring the smallest ones, are protected with a thin CdSe shell that acts as a protective spacer. However, instead of varying the spacer thickness as in the previous case, we vary the size of the PbSe core. In each case, the CdSe shell thickness is less than 0.6 nm (see Table 1 in the Supporting Information for details). Figure 4a shows the average stoichiometry attained by using of two

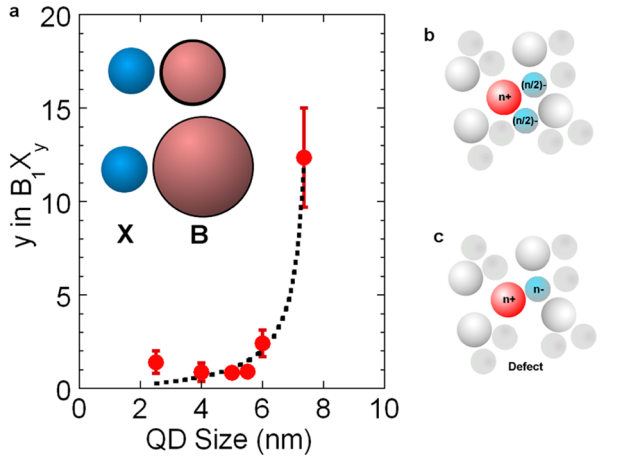

Figure 4. (a) Variation of stoichiometry of PbSe/CdSe(B) + Cu:CdS(X) QD assemblies as a function of the PbSe/CdSe QD size. (b) Schematic of AX_2 Coulomb-bound assemblies without stoichiometric defects. (c) Schematic of a stoichiometric defect where a negatively charged QD is removed and its negative charge is transferred into the other negatively charged QD at the same center.

identical Cu/CdS samples. The x axis corresponds to the total PbSe-based QD diameter, including the shell thickness. The error bars represent the range of stoichiometries observed. The Cu:CdS QDs have a radius of 2.5 nm and a 1.19% percent copper inclusion that corresponds to the presence of ∼19 copper ions per QD. For 2−5 nm PbSe/CdSe QDs, the assembly composition is observed to be nearly constant with size. Beyond a 5.5 nm size, the ability of a PbSe/CdSe QD to interact with multiple Cu:CdS QDs increases rapidly, and the number of Cu:CdS QDs rises to 12 per 7.4 nm PbSe/CdSe dot.

As shown in the Supporting Information, it is possible to show that the assembly composition is now given by $\frac{1}{E + F/r_+}$ for large deviations away from a 1:1 stoichiometry. As shown in Figure 4a, this expression provides an accurate description of the data.

The validity of the proposed thermodynamic model in accounting for the composition of QD assemblies is thus confirmed. As these assemblies lack an internal structural order but none the less represent an end product at the thermodynamic equilibrium,[36,37] these bear a stronger resemblance to liquids and glasses rather than crystalline solids. Thus, even in the absence of a microscopic structural order, the thermodynamic model presented here can readily account for the reasons behind the existence of a fixed composition. The equilibrium composition can be obtained by minimizing the energy, $\frac{\partial \Delta E_{n,1+x}}{\partial x} = 0$. While the Coulomb terms have an explicit dependence on x, the dependence of other terms such as C_{av} is implicit and expected to be weaker. This none the less enables

DOI: 10.1021/acsomega.7b01486
ACS Omega 2018, 3, 266−272

the determination of the equilibrium composition. The energy required to produce a site-specific defect by the addition or removal of one of the participating QDs is then related to

$$\Delta E_{n,1+x} - \Delta E_{n,1+x0} \approx \frac{\partial \Delta E_{n,1+x0}}{\partial x}(x - x0) + \frac{1}{2}\frac{\partial^2 \Delta E_{n,1+x0}}{\partial x^2}(x - x0)^2 = \frac{1}{2}\frac{\partial^2 \Delta E_{n,1+x0}}{\partial x^2}(x - x0)^2$$

The second energy derivative $\frac{\partial^2 \Delta E_{n,1+x0}}{\partial x^2}$ can be evaluated and contains the Coulomb interaction terms as the leading contributors (Supporting Information). This implies that $\frac{\partial^2 \Delta E_{n,1+x0}}{\partial x^2} \approx$ O (1 eV), thereby setting a strong penalty for the deviation from an optimal composition in the QD assembly.

To qualitatively illustrate this effect, consider an AX_2 solid as shown in the schematic in Figure 4b. The creation of a single AX-type stoichiometry defect requires the discharging of an X QD and further the injection of this charge into the remaining X dot. This implies that defect creation is associated with a Coulomb charging term of the form $\frac{n^2}{2cd}$ which is O (1 eV), apart from the penalties associated with changes in the local structure (Figure 4c).

CONCLUSIONS

To conclude, we examined the mechanistic principles for the formation of QD assemblies. It is found that QD assemblies formed by charge transfer between participating dots are adequately explained by equilibrium thermodynamics. Despite the apparent lack of a crystallographic structure, QD assemblies show a definite composition in terms of the ratios of participating QDs. A thermodynamic model that accounts for trends in assembly formation in QDs as a function of size and structure is developed. The model accurately explains a change in the assembly composition from 1:1.26 to 1:0.23 for ZnTe/CdS and Cu:CdS assemblies with respect to the two QDs. A different trend is observed and explained in the case of PbSe/CdSe and Cu:CdS QDs. Most unexpectedly, the magnitude of the onsite Coulomb interactions is identified to be the reason behind the existence of a fixed composition as opposed to the expected quantum confinement.

MATERIALS AND METHOD

Chemicals Used. Cadmium acetate dihydrate (Sigma-Aldrich, 98%), myristic acid (Sigma-Aldrich, 98%), selenium (Se, Sigma-Aldrich, 99.99%), tellurium (Te, SigmaAldrich, 99.99%), copper chloride dihydrate (ACS reagent, 99.8%), zinc acetate trihydrate ($Zn(CH_3COO)_2{\cdot}2H_2O$, Sigma-Aldrich, 98%), sodium borohydride ($NaBH_4$, Sigma-Aldrich, 96%), trioctylphosphine (TOP, Sigma-Aldrich, technical grade, 90%), 1-octadecene (ODE, Sigma-Aldrich, technical grade, 90%), oleylamine (technical grade, 70%), sulfur (S, Sigma-Aldrich, <99.5%), oleic acid (technical grade, Sigma-Aldrich, 90%), cadmium oxide (Sigma-Aldrich, 99.9%), and lead oxide (Alfa Aesar, 99.9%).

Hexane (AR grade, 99%), 1,4-butanediol (90%, AR), dextrose (95% anhydrous, AR), HCl (99%), and HNO_3 (98%) were purchased from SD Fine Chemicals. All chemicals were used without further purification.

PbSe Magic-Sized Nanocrystals. PbSe magic-sized nanocrystals (MSNs) were synthesized by following the established procedure.[38] Lead oxide [0.1 mmol (mmol), 0.69 g], 9.5 mmol of oleic acid (5 mL), and ODE (12 mL) were added into a 50 mL round-bottom (RB) flask, and the mixture was heated to 150 °C under argon for 1.5 h. Then, the flask was cooled down to RT, and 4 mL of 2 M TOPSe (tri-octyl phosphine selenide) was injected into the RB flask at RT. After 4 h, the solution turned brown; this indicates the formation of PbSe MSNs. Cleaned MSNs are obtained by centrifugation with methanol, ethanol, and isopropanol. The absorption spectrum of MSCNs is given in S2 (dark red solid line). Here, 2 M TOPSe was prepared by dissolving 1.248 g of Se in 8 mL of TOP.

Synthesis of Lead Selenide/Cadmium Selenide Core/Shell QDs (PbSe/CdSe). Synthesis of core/shell PbSe/CdSe QDs was done following the established procedure[39] with slight modifications.

PbSe Core. PbO (0.1 mmol, 0.69 g), 0.4 mmol (2 mL) of oleic acid, and 12 mL of ODE were added to the abovementioned RB flask. The mixture was degassed and kept in argon atmosphere. Then, the mixture was heated to 180 °C for 1.5 h with constant stirring. After 1.5 h, 4 mL of 2 M TOPSe was added to the RB flask at 180 °C. Reaction was immediately quenched by adding 10 mL of toluene once we achieved the desired size. PbSe QDs were purified by multiple centrifugations with methanol, ethanol, and isopropanol.

CdSe Shell on the PbSe Core. PbSe QDs obtained from the abovementioned step were dispersed in 10 mL of toluene in an RB flask. About 10 mL of 0.1 mmol cadmium oleate was added, and then the flask was kept under argon atmosphere at 100 °C for 1 h with constant stirring. Reaction was quenched by reducing the temperature, and the PbSe/CdSe QD precipitate was collected by centrifuging with methanol, ethanol, and isopropanol. The absorption spectra of PbSe/CdSe QDs (S2a) and the TEM image (S2b) are given in Figure S2. The information regarding size of PbSe-based QDs used in assembly preparation is given in Table 1 (Supporting Information).

Synthesis of ZnTe/CdS. Synthesis of the ZnTe/CdS core/shell was done following the previously reported method.[19]

ZnTe Core. *Synthesis of ZnTe Cores Involving Two Steps.* The first step involves making a reactive telluride ion precursor by treating 0.5 mmol of tellurium with reducing agents such as $NaBH_4$ in this case, with 2 mL of 1,4-butanediol as solvent at 60 °C under argon atmosphere for 5 min. Then, 0.1 mmol of dextrose was dissolved in 1 mL 1,4-butanediol which was added to consume excess borohydride.

In the second step, 0.5 mmol (92 mg) of zinc acetate dihydrate was heated in another flask at 100 °C with 4 mL of ODE and 1 mL of oleylamine. Once the temperature of flask reached 100 °C, the contents the flask described in step 1 were rapidly injected.

CdS Shell. Cd-oleate and S in oleylamine were added dropwise into the flask containing the ZnTe core at 230 °C under argon atmosphere, until the desired shell thickness on the core was obtained. Aliquots were collected to obtain the desired shell thickness. The graph showing absorption spectra of ZnTe/CdS QDs is given in the Supporting Information (Figure S3).

Synthesis of Cu-Doped Cadmium Sulphide (Cu:CdS). Synthesis of Cu:CdS QDs was done following a procedure reported in the literature.[40] Copper chloride dihydrate (3 mg) and 0.1 mmol of sulfur (3.2 mg) were added to 0.1 mmol of cadmium myristate with 3 mL of ODE, and then reaction

DOI: 10.1021/acsomega.7b01486
ACS Omega 2018, 3, 266−272

mixture was heated up to 230 °C under argon atmosphere. Once the temperature reached 230 °C, 1 mL of oleylamine was injected dropwise into the reaction mixture. Around 1.19% of doping was observed in all our cases. Immediately, the reaction was quenched by removing the heating mantle. Cu:CdS QDs were collected by centrifuging with methanol, ethanol, and isopropanol. The absorption and photoluminescence spectra of cleaned Cu:CdS are given in the Supporting Information (Figure S4).

Synthesis of Cu-Doped ZnSe/CdSe (Cu:ZnSe/CdSe). Cu−ZnSe/CdSe QDs were synthesized by a procedure reported in the literature.[41]

Zinc acetate (0.1 mmol), 4 mL of ODE, 1 mL of oleylamine, and 3 mg of $CuCl_2$ were added to a three-necked RB flask and heated to 180 °C under argon atmosphere for 2 min. About 0.5 mL of 0.1 mmol TOPSe was injected rapidly into the flask at 180 °C for nucleation. For growth, 1.5 mL of 0.1 mmol TOPSe was injected dropwise at 180 °C, and about 0.2 mL of 0.1 mmol Cd-oleate was injected. The resultant Cu:ZnSe/CdSe QDs were collected and purified.

The absorption and photoluminescence spectrum of cleaned Cu:ZnSe/CdSe is given in the Supporting Information (Figure S5).

Synthesis of QD Assemblies. Synthesis of QD assemblies was done by following a previously reported method.[20] Formation of QD assemblies involves reaction between two different QDs: one is X (X = Cu:CdS) and the other is A or B (A = ZnTe/CdS B = PbSe/CdSe).

A known amount of QD X and QD A or QD B was dispersed separately in 0.5 mL hexane each. After that, QD X is mixed with QD A or B and allowed to dry completely. After complete evaporation of hexane in the mixture, about 0.5 mL of hexane was again added and kept for evaporation. The addition of solvent and evaporation of the solvent was repeated 5 times. This process increases the number of collisions between the dots in the mixture. Electrons are transferred between QDs during QD−QD collisions. As a result, X gains a negative charge, and QD A or B acquires a positive charge, setting up a Columbic force of attraction between them. Because of the Columbic force of attraction, bound QDs precipitate from solution, giving rise to assemblies. The assembly precipitate was separated from unreacted QDs by centrifugation. The precipitate was washed thoroughly with hexane to eliminate unbound QDs. This purified assembly is used for further analysis. The same procedure is carried out for all the sizes of QD A and QD B. TEM and high-resolution TEM images of various QD assemblies are given in the Supporting Information (Figure S1).

■ ASSOCIATED CONTENT

Supporting Information

The Supporting Information is available free of charge on the ACS Publications website at DOI: 10.1021/acsomega.7b01486.

Optical characterization, TEM images, sizes of PbSe/CdSe samples, equations used to fit data (PDF)

■ AUTHOR INFORMATION

Corresponding Author

*E-mail: anshup@iisc.ac.in (A.P.).

ORCID

Anshu Pandey: 0000-0003-3195-1522

Author Contributions

The manuscript was written through contributions of all authors. All authors have given approval to the final version of the manuscript.

Notes

The authors declare no competing financial interest.

■ ACKNOWLEDGMENTS

R.M. thanks the Council of Scientific and Industrial Research for financial support. A.P. thanks the Indian Institute of Science and the Department of Science and Technology for generous funding.

■ ABBREVIATIONS

QD, quantum dot; HRTEM, high resolution transmission electron micrograph; TEM, transmission electron micrograph

■ REFERENCES

(1) Nguyen, D.; Nguyen, H. A.; Lyding, J. W.; Gruebele, M. Imaging and Manipulating Energy Transfer Among Quantum Dots at Individual Dot Resolution. *ACS Nano* **2017**, *11*, 6328−6335.

(2) Akkerman, Q. A.; D'innocenzo, V.; Accornero, S.; Scarpellini, A.; Petrozza, A.; Prato, M.; Manna, L. Tuning the Optical Properties of Cesium Lead Halide Perovskite Nanocrystals by Anion Exchange Reactions. *J. Am. Chem. Soc.* **2015**, *137*, 10276−10281.

(3) Ekimov, A. I.; Kudryavtsev, I. A.; Efros, A. L.; Yazeva, T. V.; Hache, F.; Schanne-Klein, M. C.; Rodina, A. V.; Ricard, D.; Flytzanis, C. Absorption and Intensity-Dependent Photoluminescence Measurements on CdSe Quantum Dots: Assignment of the First Electronic Transitions. *J. Opt. Soc. Am. B* **1993**, *10*, 100−107.

(4) Lorenzon, M.; Pinchetti, V.; Bruni, F.; Bae, W. K.; Meinardi, F.; Klimov, V. I.; Brovelli, S. Single-Particle Ratiometric Pressure Sensing Based on "Double-Sensor" Colloidal Nanocrystals. *Nano Lett.* **2017**, *17*, 1071−1081.

(5) Kershaw, S. V.; Rogach, A. L. Infrared Emitting HgTe Quantum Dots and Their Waveguide and Optoelectronic Devices. *Z. Phys. Chem.* **2015**, *229*, 23−64.

(6) Dong, Y.; Choi, J.; Jeong, H.-K.; Son, D. H. Hot Electrons Generated from Doped Quantum Dots via Upconversion of Excitons to Hot Charge Carriers for Enhanced Photocatalysis. *J. Am. Chem. Soc.* **2015**, *137*, 5549−5554.

(7) Whitham, K.; Yang, J.; Savitzky, B. H.; Kourkoutis, L. F.; Wise, F.; Hanrath, T. Charge Transport and Localization in Atomically Coherent Quantum dot Solids. *Nat. Mater.* **2016**, *15*, 557−563.

(8) Otto, T.; Miller, C.; Tolentino, J.; Liu, Y.; Law, M.; Yu, D. Gate-Dependent Carrier Diffusion Length in Lead Selenide Quantum Dot Field-Effect Transistors. *Nano Lett.* **2013**, *13*, 3463−3469.

(9) Xiao, R.; Hou, Y.; Fu, Y.; Peng, X.; Wang, Q.; Gonzalez, E.; Jin, S.; Yu, D. Photocurrent Mapping in Single-Crystal Methylammonium Lead Iodide Perovskite Nanostructures. *Nano Lett.* **2016**, *16*, 7710−7717.

(10) Kang, I.; Wise, F. W. Electronic structure and optical properties of PbS and PbSe quantum dots. *J. Opt. Soc. Am. B* **1997**, *14*, 1632−1646.

(11) Bronstein, N. D.; Yao, Y.; Xu, L.; O'Brien, E.; Powers, A. S.; Ferry, V. E.; Alivisatos, A. P.; Nuzzo, R. G. Quantum Dot Luminescent Concentrator Cavity Exhibiting 30-Fold Concentration. *ACS Photonics* **2015**, *2*, 1576−1583.

(12) Caruge, J. M.; Halpert, J. E.; Wood, V.; Bulović, V.; Bawendi, M. G. Colloidal Quantum-Dot Light-Emitting Diodes with Metal-Oxide Charge Transport Layers. *Nat. Photonics* **2008**, *2*, 247−250.

(13) Chanyawadee, S.; Harley, R. T.; Henini, M.; Talapin, D. V.; Lagoudakis, P. G. Photocurrent Enhancement in Hybrid Nanocrystal Quantum-Dot P−I−N Photovoltaic Devices. *Phys. Rev. Lett.* **2009**, *102*, 077402.

(14) Shim, M. Colloidal Nanorod Heterostructures for Photovoltaics and Optoelectronics. *J. Phys. D: Appl. Phys.* **2017**, *50*, 173002−173018.

DOI: 10.1021/acsomega.7b01486
ACS Omega 2018, 3, 266−272

(15) Dillen, D. C.; Kim, K.; Liu, E.-S.; Tutuc, E. Radial Modulation Doping in Core−Shell Nanowires. *Nat. Nanotechnol.* **2014**, *9*, 116−120.
(16) Schimpf, A. M.; Thakkar, N.; Gunthardt, C. E.; Masiello, D. J.; Gamelin, D. R. Charge-Tunable Quantum Plasmons in Colloidal Semiconductor Nanocrystals. *ACS Nano* **2014**, *8*, 1065−1072.
(17) Viswanatha, R.; Brovelli, S.; Pandey, A.; Crooker, S. A.; Klimov, V. I. Copper-Doped Inverted Core/Shell Nanocrystals with "Permanent" Optically Active Holes. *Nano Lett.* **2011**, *11*, 4753−4758.
(18) Mahadevu, R.; Kaur, H.; Pandey, A. Hidden role of anion exchange reactions in nucleation of colloidal nanocrystals. *CrystEngComm* **2016**, *18*, 759−764.
(19) Mahadevu, R.; Yelameli, A. R.; Panigrahy, B.; Pandey, A. Controlling Light Absorption in Charge-Separating Core/Shell Semiconductor Nanocrystals. *ACS Nano* **2013**, *7*, 11055−11063.
(20) Mahadevu, R.; Pandey, A. Ionic Bonding between Artificial Atoms. *J. Phys. Chem. C* **2014**, *118*, 30101−30105.
(21) Guyot-Sionnest, P. Electrical Transport in Colloidal Quantum Dot Films. *J. Phys. Chem. Lett.* **2012**, *3*, 1169−1175.
(22) Sacanna, S.; Pine, D. J.; Yi, G.-R. Engineering Shape: the Novel Geometries of Colloidal Self-Assembly. *Soft Matter* **2013**, *9*, 8096−8106.
(23) Yi, G.-R.; Thorsen, T.; Manoharan, V. N.; Hwang, M.-J.; Jeon, S.-J.; Pine, D. J.; Quake, S. R.; Yang, S.-M. Generation of Uniform Colloidal Assemblies in Soft Microfluidic Devices. *Adv. Mater.* **2003**, *15*, 1300−1304.
(24) Lee, V.; Waitukaitis, S. R.; Miskin, M. Z.; Jaeger, H. M. Direct observation of particle interactions and clustering in charged granular streams. *Nat. Phys.* **2015**, *11*, 733−737.
(25) Peters, I. R.; Jaeger, H. M. Quasi-2D Dynamic Jamming in Cornstarch Suspensions: Visualization and Force Measurements. *Soft Matter* **2014**, *10*, 6564−6570.
(26) van Anders, G.; Klotsa, D.; Karas, A. S.; Dodd, P. M.; Glotzer, S. C. Digital Alchemy for Materials Design: Colloids and Beyond. *ACS Nano* **2015**, *9*, 9542−9553.
(27) Yi, G.-R.; Manoharan, V. N.; Michel, E.; Elsesser, M. T.; Yang, S.-M.; Pine, D. J. Colloidal Clusters of Silica or Polymer Microspheres. *Adv. Mater.* **2004**, *16*, 1204−1208.
(28) Boal, A. K.; Ilhan, F.; DeRouchey, J. E.; Thurn-Albrecht, T.; Russell, T. P.; Rotello, V. M. Self-assembly of nanoparticles into structured spherical and network aggregates. *Nature* **2000**, *404*, 746−748.
(29) Li, M.; Schnablegger, H.; Mann, S. Coupled synthesis and self-assembly of nanoparticles to give structures with controlled organization. *Nature* **1999**, *402*, 393−395.
(30) Grzelczak, M.; Vermant, J.; Furst, E. M.; Liz-Marzán, L. M. Directed Self-Assembly of Nanoparticles. *ACS Nano* **2010**, *4*, 3591−3605.
(31) Tripp, S. L.; Pusztay, S. V.; Ribbe, A. E.; Wei, A. Self-Assembly of Cobalt Nanoparticle Rings. *J. Am. Chem. Soc.* **2002**, *124*, 7914−7915.
(32) Rabani, E.; Reichman, D. R.; Geissler, P. L.; Brus, L. E. Drying-mediated self-assembly of nanoparticles. *Nature* **2003**, *426*, 271−274.
(33) Jiang, Z.; He, J.; Deshmukh, S. A.; Kanjanaboos, P.; Kamath, G.; Wang, Y.; Sankaranarayanan, S. K. R. S.; Wang, J.; Jaeger, H. M.; Lin, X.-M. Subnanometre Ligand-Shell Asymmetry Leads to Janus-Like Nanoparticle Membranes. *Nat. Mater.* **2015**, *14*, 912−917.
(34) Kanjanaboos, P.; Lin, X.-M.; Sader, J. E.; Rupich, S. M.; Jaeger, H. M.; Guest, J. R. Self-Assembled Nanoparticle Drumhead Resonators. *Nano Lett.* **2013**, *13*, 2158−2162.
(35) Landau, L. D.; Lifshitz, E. M. *Course of Theoretical Physics—Statistical Physics Part 2*; Elsevier: New York, 2011; Vol. *9*.
(36) Colón-Meléndez, L.; Beltran-Villegas, D. J.; van Anders, G.; Liu, J.; Spellings, M.; Sacanna, S.; Pine, D. J.; Glotzer, S. C.; Larson, R. G.; Solomon, M. J. Binding Kinetics of Lock and Key Colloids. *J. Chem. Phys.* **2015**, *142*, 174909−174918.
(37) Goodrich, C. P.; Dagois-Bohy, S.; Tighe, B. P.; van Hecke, M.; Liu, A. J.; Nagel, S. R. Jamming in Finite Systems: Stability, Anisotropy, Fluctuations, and Scaling. *Phys. Rev. E: Stat., Nonlinear, Soft Matter Phys.* **2014**, *90*, 022138.
(38) Evans, C. M.; Guo, L.; Peterson, J. J.; Maccagnano-Zacher, S.; Krauss, T. D. Ultrabright PbSe Magic-sized Clusters. *Nano Lett.* **2008**, *8*, 2896−2899.
(39) Pietryga, J. M.; Werder, D. J.; Williams, D. J.; Casson, J. L.; Schaller, R. D.; Klimov, V. I.; Hollingsworth, J. A. Utilizing the Lability of Lead Selenide to Produce Heterostructured Nanocrystals with Bright, Stable Infrared Emission. *J. Am. Chem. Soc.* **2008**, *130*, 4879−4885.
(40) Grandhi, G. K.; Viswanatha, R. Tunable Infrared Phosphors Using Cu Doping in Semiconductor Nanocrystals: Surface Electronic Structure Evaluation. *J. Phys. Chem. Lett.* **2013**, *4*, 409−415.
(41) Grandhi, G. K.; Tomar, R.; Viswanatha, R. Study of Surface and Bulk Electronic Structure of II−VI Semiconductor Nanocrystals Using Cu as a Nanosensor. *ACS Nano* **2012**, *6*, 9751−9763.

DOI: 10.1021/acsomega.7b01486
ACS Omega 2018, 3, 266−272